

PAPER

Pilot study on numerical prediction of sound reduction index of double window system: Comparison of finite element prediction method with measurement

Marie Mimura^{1,*}, Takeshi Okuzono^{2,†} and Kimihiro Sakagami^{2,‡}

¹*Technology and Innovation Center, YKK Corporation,
200, Yoshida, Kurobe, 938–8601 Japan*

²*Environmental Acoustical Laboratory, Department of Architecture,
Graduate School of Engineering, Kobe University,
1–1 Rokkodai, Nada-ku, Kobe, 657–8501 Japan*

(Received 1 April 2021, Accepted for publication 7 September 2021)

Abstract: The development of windows with high sound insulation performance is essential for preventing the infiltration of traffic noise and the leakage of room noise. A numerical prediction is an effective means of reducing sound insulation testing and development costs to develop a quietness window. As a numerical prediction method for the sound reduction index, the finite element method (FEM) is useful in dealing with structure-acoustic problems. This study was conducted as a pilot study toward developing an accurate numerical model to predict the sound reduction index of a double window. We discussed the accuracy of an FEM model for predicting the diffuse incidence sound reduction index of double windows through a comparison with measured values for a simplified realistically scaled double window. The FE results were compared with measured ones for eight cases with and without a frame absorber. Results showed that the best match to measured values is obtained when using a frame absorber in all the perimeters inside the air cavity. Also, a better agreement is obtained at frequencies of 160–2,000 Hz in other cases. However, a marked discrepancy is found at frequencies above 2,000 Hz and below 160 Hz. Possible reasons for the discrepancies are also discussed.

Keywords: Sound insulation, Sound reduction index, Finite element method, Double window

1. INTRODUCTION

The sound environment in dwellings has long been of great interest and has been studied extensively [1]. Sound insulation is essential for preventing the infiltration of outdoor noise such as traffic noise into indoor living spaces and for protecting privacy and preventing the leakage of sound to the outside. Generally, windows are desirable for higher sound insulation performance because they have lower sound insulation performance than other building materials, such as concrete, for a wall. The most realistic means of achieving high sound insulation with a window is to use a double window comprising two glass panels and two sashes. At high frequencies, double windows can offer better sound insulation performance than a single window. However, the sound insulation performance of double

windows becomes lower than that of a single window at low frequencies owing to the mass–air–mass resonance. To develop windows with high sound insulation performance, one must elucidate the mechanisms of sound insulation in window systems and understand the design parameters that affect the sound insulation performance of various window types.

Generally, the sound insulation performance of windows is evaluated using a test following a standard such as ISO 10140 [2]. However, during the development of high-sound insulation windows, numerical analyses are beneficial for obtaining a design guideline because the sound insulation test has some difficulties. First, it requires much time and cost for a detailed study of sound transmission phenomena. It also has difficulty with uncertainty. The repeatability of measurements can often be degraded because of differences in the construction accuracy of specimen edges of test room walls and the different degrees of air leakage at the specimen mounting part [3–5]. Furthermore, the sound insulation performance of windows

*e-mail: m-mimura@ykk.com

†e-mail: okuzono@port.kobe-u.ac.jp

‡e-mail: saka@kobe-u.ac.jp

[doi:10.1250/ast.43.32]

is likely to change according to individual differences derived from differences in the degree of glass edge mounting to sashes, in the damping degree of glass, and in air gap arising from poor construction [6–8]. Numerical analyses can control such factors more easily than in experiments within a given physical model.

Double windows have the same sound insulation mechanism as double walls. Many theoretical models have been presented to predict the sound insulation performance of double walls [9–11]. However, they have various limitations in predicting the sound insulation mechanisms of existing windows, such as modeling under fixed conditions, panel size effects, and sound-incidence conditions. Therefore, theoretical predictions are sometimes insufficient for obtaining accurate prediction, although continuous efforts [12–14] are still being made to increase the prediction accuracy. Numerical analysis enables us to model the detailed conditions crucial for modeling real windows. Finite element (FE) analysis is a suitable choice because it can deal with structure-acoustic problems.

In recent years, the sound insulation performance of double walls has been predicted in many studies [15–20] by FE analysis. However, in most studies, only the performance in the low-frequency range was specifically examined. Although Arjunan *et al.* [15] calculated the sound reduction index by FE analysis with the frequency-dependent Rayleigh damping matrix at frequencies of 100 to 3,150 Hz, the dimensions of numerical models are not realistic. These unrealistic models might derive from the high computation costs of FE analysis with a realistic double wall model in a broad frequency range. Poblet-Puig *et al.* [18] studied the effects of wall dimensions, support conditions, and spring support stiffness by FE analysis up to 5,000 Hz, but the consistency with the actual measurements remains unclear because of the lack of comparison with experimentally obtained results.

Moreover, the FE prediction of the sound insulation performance of double windows has attracted much less attention than that of double walls. Løvholt *et al.* [20] demonstrated the importance of modeling in the structural connection between different building elements such as sheets, studs, and windows through the calculation of sound reduction index of real-scale lightweight walls with a window at very low frequencies below 100 Hz. Soussi *et al.* [21] calculated the sound reduction index of double-glazed windows with a simplified window frame at frequencies of 100–500 Hz. Similarly to that of double walls, the FE prediction of double windows has been conducted only at low frequencies. Therefore, the accuracy of FE prediction with a realistic scale model for a broad frequency range has remained unclear.

This study was conducted as a pilot study toward developing an accurate numerical model to predict the

sound reduction index of a double window. We will discuss the prediction capability of FE method (FEM) modeling for computing the diffuse incidence sound reduction index of double windows in a wide frequency range. As the first step of the research, we selected a simple double window model instead of a real double window to keep the system as simple as possible. The sound reduction indices of the simple window model obtained from a vibroacoustic FE model and measurement values were compared for eight cases in total with and without a frame absorber, that is, porous sound-absorbing materials, placed along the inner cavity perimeter.

2. EXPERIMENTAL OUTLINE FOR COMPARISON

For comparison with the FE results explained in Sect. 3, we used measured results for the simplified double window model introduced in an earlier work [22]. In the earlier study, the sound reduction indices and sound pressure levels (SPL) in an inner air cavity for cases with and without a frame absorber were measured using the double window model. The measurements were taken in a reverberant room and a hemi-anechoic chamber in accordance with JIS A 1441-1 [23], which is comparable to ISO 15186-1:2000 [24]. The source-reverberant room has a volume of 36.9 m³. For the reader's convenience, the model and experimental conditions are described in detail below.

2.1. Details of Simplified Double Window Model

Figure 1 shows the details of the double window model, which comprises two acrylic panels, wooden frames, rubber sheets, and wooden block part or glass wool. Note that the glass wool was used only for the frame absorber cases described in Sect. 2.2. The acrylic panels have dimensions of 1,158 mm × 1,159 mm × 5 mm. The distance between the two panels, i.e., air cavity depth, is 90 mm. The inner air cavity has a size of 800 mm × 800 mm × 90 mm and is surrounded by the two acrylic panels, rubber sheets, and wooden block part or glass wool. The wooden frame is 80 mm thick with widths of 75 mm, 84 mm, 79.5 mm, and 79.5 mm on the upper, lower, left, and right sides, respectively. The sizes of wooden block and glass wool parts differ depending on the conditions, which is explained in Sect. 2.2. The rubber sheet was inserted between the acrylic panels and the assembly parts composed of the wooden frame and the wooden block part or the glass wool. The rubber sheets for air sealing are 5 mm thick with widths of 175 mm, 184 mm, 179.5 mm, and 179.5 mm on the upper, lower, left, and right sides, respectively, as shown in Fig. 1. The acrylic panels, rubber sheets, and wooden frames were fixed with bolts at 32 positions, as shown in Fig. 1. The double window model

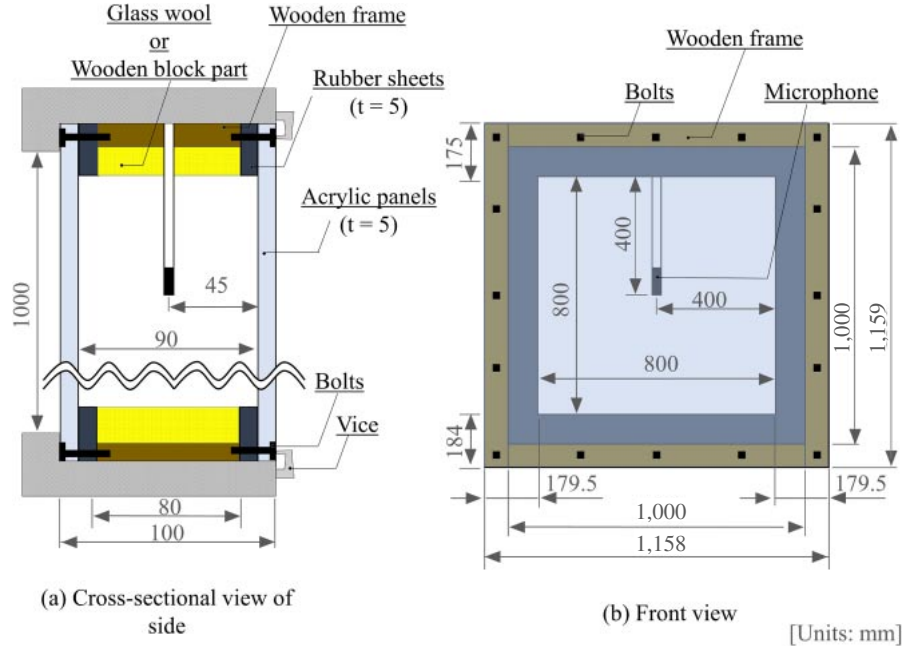


Fig. 1 Appearance of double window model [22].

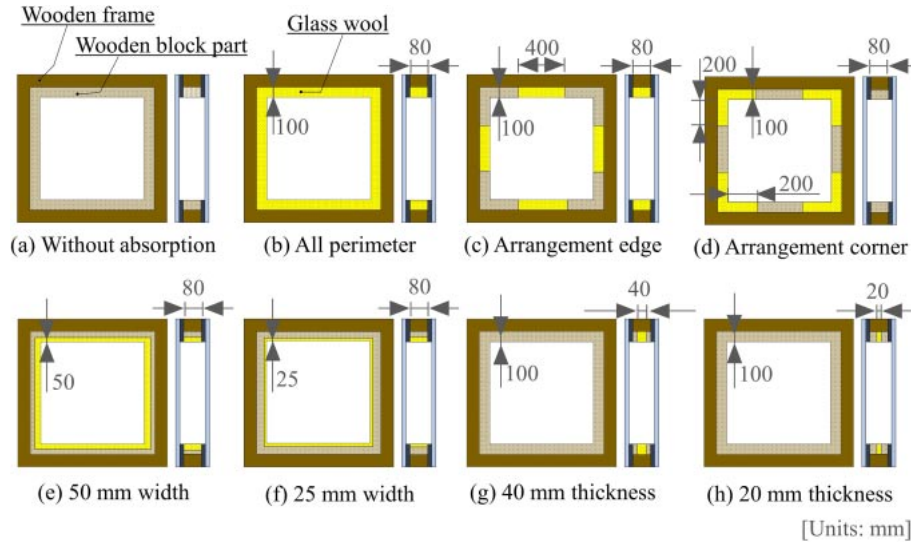


Fig. 2 Absorption installation conditions (cross-sectional views of front and side) [22].

was attached to the wall with a vice near the edge of the panels. The gaps between the specimen and the walls were filled with clay.

The mass–air–mass resonance frequency f_{rmd} of the experimental double window model is approximately calculated using the theory for an infinite double-leaf wall [25] as

$$f_{\text{rmd}} = \frac{1}{2\pi} \sqrt{\frac{m_1 + m_2}{m_1 \cdot m_2} \cdot \frac{\rho c^2}{d}}, \quad (1)$$

where f_{rmd} stands for the mass–air–mass resonance frequency, m_1 and m_2 respectively represent the surface density of the two panels (kg/m^2), ρ denotes the density of

air ($1.2 \text{ kg}/\text{m}^3$), c expresses the speed of sound in air (340 m/s), and d signifies the air cavity depth. The computed resonance frequency is 114 Hz .

2.2. Measurement Conditions

The sound reduction indices of the double window and SPLs in the inner air cavity were measured for eight cases. One is a case with no frame absorber, denoted by “without absorption,” as shown in Fig. 2(a). The other seven cases have glass wool at different locations along the perimeter of the inner air cavity, as shown in Figs. 2(b)–2(h). These seven cases are classified broadly into four groups: “All perimeter,” “Arrangement,” “Thickness,” and “Width.”

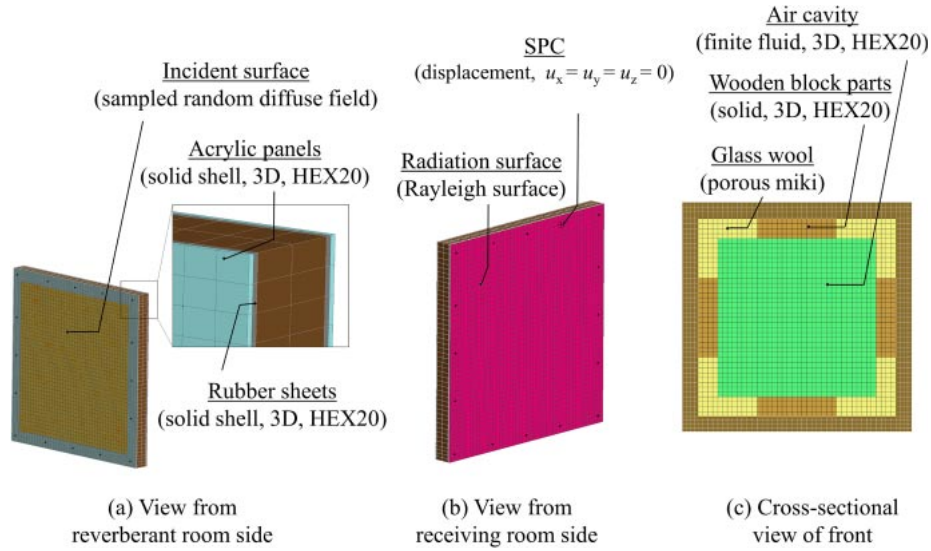


Fig. 3 Finite element model of “Arrangement corner” for low frequency.

In the “All perimeter” case, the wooden block part in the “Without absorption” case was replaced with 100-mm-wide glass wool along the entire perimeter. In the “Arrangement” cases in Figs. 2(c) and 2(d), we consider two measurement conditions with absorption at different positions. In both cases, the width of glass wool is 100 mm. In the “Edge” case in Fig. 2(c), glass wool of 400 mm length is installed at the center of each of the four sides. In the “Corner” case in Fig. 2(d), glass wool of 200 mm length is installed at each corner. In both cases, the wooden block part remains at the locations not replaced with glass wool. In the “Width” cases in Figs. 2(e) and 2(f), glass wool pieces with widths of 50 and 25 mm are installed, respectively. To keep the volumes of the air cavity equal in all cases, wooden block part with widths of 50 and 75 mm are installed behind the glass wool, respectively. In the “Thickness” cases in Figs. 2(g) and 2(h), glass wool with width of 100 mm and thickness of 40 and 20 mm, respectively, is inserted along the entire perimeter. To keep the air cavity depth constant at 90 mm, wooden block part with thickness of 20 and 30 mm are installed between the glass wool and the panels, respectively.

SPLs were measured at the microphone position in the air cavity shown in Fig. 1, and they are also used for comparison with FE results.

3. FINITE ELEMENT MODEL AND SETUP OF ANALYSIS

Commercial vibroacoustic FEM simulation software, namely, ACTRAN 2020, was used to predict the sound reduction indices of the double window model. A linear direct frequency response simulation was performed to validate the simulated FE results over a broad frequency range. The calculated results of the sound reduction index

and SPL in the inner air cavity were compared with measured values at one-third-octave band center frequencies of 100–5,000 Hz. Note that FE analyses were performed at 1/24-octave band center frequencies in the frequency range of 90 Hz to 5.6 kHz. Then, the sound reduction index was calculated as a 1/3-octave band value. Figure 3 shows the FE model of the double window presented in Fig. 1. As shown in the Fig. 3, only the double window part was discretized with finite elements to keep the computational cost within a manageable level at the high frequency, i.e., the source reverberant and receiving rooms were not discretized with finite elements. Receiving points for SPL comparison in the inner air cavity were placed at the center of the cavity, that is, the same position of measurement as that in Fig. 1.

A sparse direct solver called MUMPS was used for solving the linear system of equations at each frequency efficiently.

3.1. Finite Elements for Spatial Discretization

For structural domains, the governing equation is the differential equation of motion for a continuum body assuming small deformation. The acrylic panels and rubber sheets were discretized by three-dimensional HEX20, i.e., twenty-node hexahedron, solid shell elements [26] with three degrees of freedom at each node for the displacements u_x , u_y , and u_z in x -, y -, and z -axes. A solid shell element is a unique element in Actran that is not a general 2D shell element. We opted to use unique elements because they do not cause either thickness locking or shear locking effects [26]. Note that although we can also select 2D shell elements for thin solid materials, the second-order elements are available for only solid shell elements. We considered that they would be more accurate in high-

frequency ranges than the first-order 2D shell elements. For acrylic panels and rubber sheets, the number of divisions in the thickness direction is one. The wooden frame and wooden block part were discretized by 3D HEX20 solid elements [27] with three degrees of freedom at each node for displacement. Note that the wooden frame and wooden block part were treated as a unit because the same material was used. The inner air cavity was discretized by 3D HEX20 fluid elements [28], solving the lossless Helmholtz equation with real wavenumbers. The glass wool was also discretized by 3D HEX20 fluid elements solving the Helmholtz equation with complex wavenumbers, considering a rigid-frame isotropic equivalent-fluid model [29,30]. For the fluid properties of the glass wool, we used the Miki model [31] to calculate the characteristic impedance and propagation constant with a flow resistivity of $13,918 \text{ Pa}\cdot\text{s}/\text{m}^2$. The discretization of support condition (SPC) was used as instead of bolts. The SPC condition is explained in detail in Sect. 3.2.

Regarding the coupling conditions, continuity in pressure and particle velocity is ensured at the interface between the two acoustic domains. At the interface between the two structural domains, continuity in stress and structural displacement is ensured. At the acoustic and structure interface, continuity in pressure and normal displacement is ensured.

For efficient calculation, we used six FE meshes with different spatial resolutions in accordance with the calculated frequency. The element size was selected to satisfy three elements per wavelength for the acoustic domain. This corresponds to six nodes per wavelength, which is known to be the rule of thumb for second-order elements. For all structural domains, the criterion of five elements per wavelength in bending waves of the acrylic panels is satisfied. The numbers of nodes in the resulting FE meshes range from 95,000 to 200,000. Note that, for the analysis in the 5,000 Hz range, the created FE mesh has only 200,000 nodes.

3.2. Boundary Conditions

Instead of modeling the source reverberant room, we used an Actran component, namely, the sampled random diffuse field [26] to the sound incident surface as in Fig. 3(a), whereby the random pressure load was applied to the acrylic panel surface on the incident field side to reproduce the diffuse incidence condition. A pressure load with a random initial phase was applied to the surface. The maximum sound incident angle considered here is 90 degrees. The incident power W_{inc} was calculated from spatial correlation on the surface. The transmitted field in the receiving room was modeled with a Rayleigh surface [26]. The radiation power W_{rad} was calculated from the surface vibration velocity based on Rayleigh's boundary

integral. The sound reduction index R was calculated as shown below,

$$R = 10 \log_{10} \left(\frac{W_{\text{inc}}}{W_{\text{rad}}} \right). \quad (2)$$

Ten samples of the sampled random diffuse field were given to the incident surface, and R was calculated from the energy average of the reduction indices of the ten samples. Regarding the effect of the number of samples, we chose to use ten samples in accordance with the resulting of the preliminary study, as shown in the appendix. When the energy average of 100 samples is taken as the true value, the variation in the average of ten samples is about $\pm 0.5 \text{ dB}$.

At the surface of the wooden frame and wooden block part, we assigned the acoustic admittance shown in the literature [32]. Note that the bolts were represented with clamped boundary conditions for solid shell elements where the three displacements were set to be zero, i.e., $u_x = u_y = u_z = 0$ [26], at all 32 nodes of the bolt positions.

3.3. Material Properties

For reliable simulations, it is essential to give an accurate loss factor of materials. We used the measured loss factors in FE analyses. For the loss factor of acrylic panels, we conducted free-support hammer testing. The tested plate has dimensions of $250 \text{ mm} \times 579 \text{ mm} \times 5 \text{ mm}$. The resulting loss factor estimated from the width of the resonance peak $\Delta f \text{ Hz}$ at 3 dB below resonance is 0.06. Although this value was obtained by averaging the loss factors up to 500 Hz, we used it for all frequency bands assuming that the loss factor is the same in the entire frequency range. The loss factor of rubber sheets evaluated using a viscoelastic spectrometer (DMS6100; Seiko Instruments Inc.) is 0.2. The loss factor of the wooden frame is 0.05, which is the value from the Actran material library. The material properties used for FE analysis are summarized in Table 1.

Table 1 Material properties.

	Young's modulus $E \text{ [Pa]}$	Poisson's ratio	Density $\rho \text{ [kg/m}^3\text{]}$	Loss factor η
Acrylic panel	3.1E+09	0.35	1,200	0.06
Wood (frame and blocks)	3.8E+09	0.3	750	0.05
Rubber sheets	1.3E+07	0.48	890	0.2
		Sound speed $[\text{m/s}]$	Air density $\rho \text{ [kg/m}^3\text{]}$	
Air cavity		340	1.225	

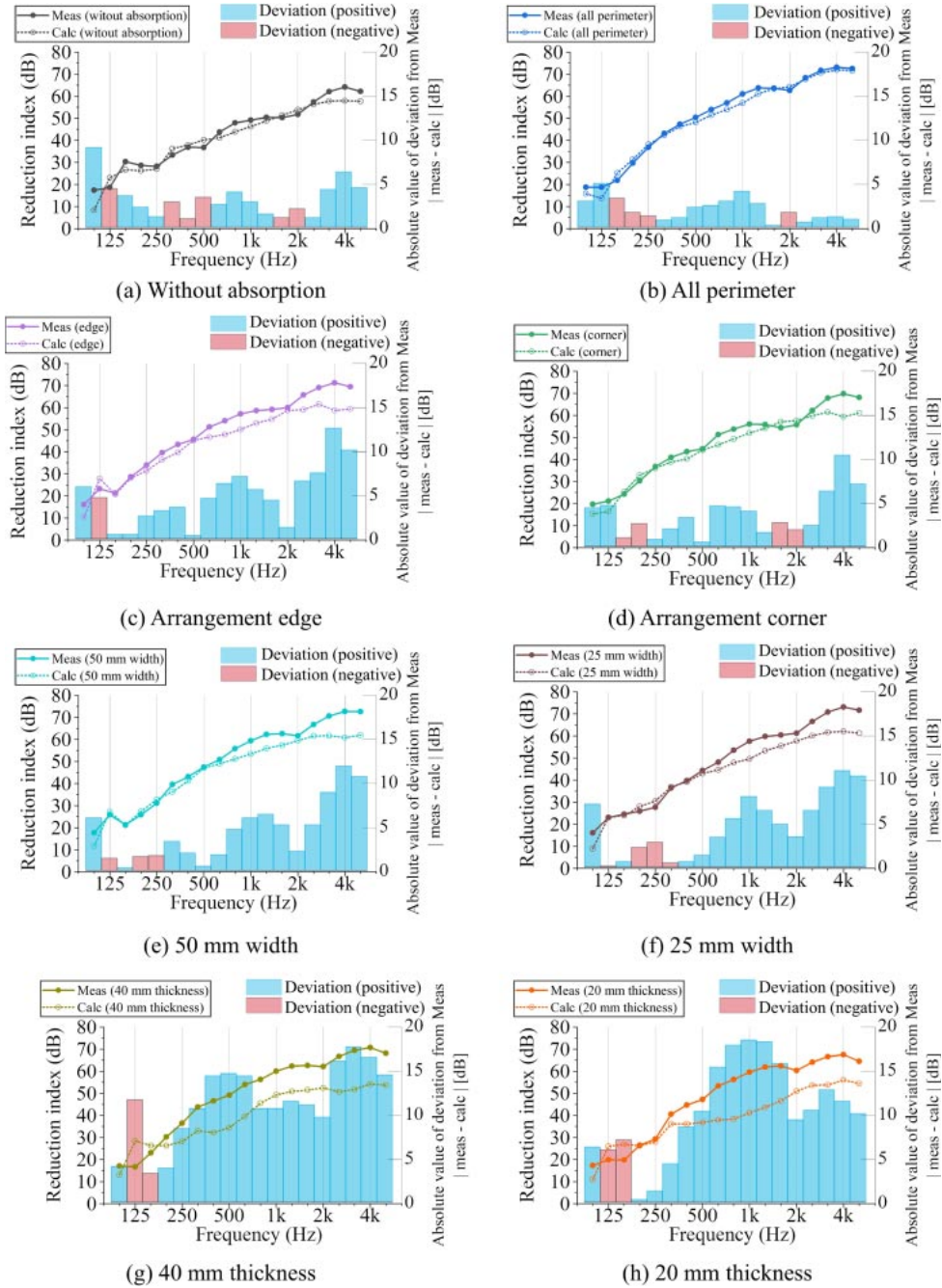


Fig. 4 Sound reduction indices of FEM and measured results for eight cases. The absolute difference is also plotted.

4. RESULTS AND DISCUSSION

Figures 4(a)–4(h) show sound reduction indices obtained by FE analysis and measurement for the eight conditions and their absolute difference for quantitative evaluation. For all cases, the minimum sound transmission, considered to be a sound dip by mass–air–mass resonance, was found at 100 or 125 Hz for FE and measured results, respectively. At frequencies higher than the resonance frequency, the sound reduction index increases with the frequency in both FE and measured results. Therefore, the frequency characteristics of the sound reduction index are

qualitatively similar. For quantitative evaluation, the best fit was obtained for the “All perimeter” case with an absolute error of less than 5 dB, where the average absolute error over frequency was 2.0 dB. Also, for the cases of “Without,” “Arrangement,” and “Width,” FE results agree well with measured results in a limited frequency range of 160–2,000 Hz with the absolute error of less than 8 dB, where the average absolute error was 2.1–3.3 dB. For these cases, the agreement is degraded for frequencies higher than 2,000 Hz, where the sound reduction indices determined by FE analysis are lower than the measured values. The worst agreements were in the case of “Thickness,” as

can be seen in Figs. 4(g) and 4(h), where the discrepancy from the measured values exceeded 10 dB. The average discrepancy was 10.3–11.3 dB. Because the cases other than the “All perimeter” case have an additional wooden block part in the perimeter of the inner air cavity, as presented in Fig. 2, the modeling of this part seems to be the cause of the poor agreement. At low frequencies below 160 Hz, the discrepancy of the FE results from the measured values exceeded 5 dB on average.

We consider the reason for the large discrepancy in the case of “Thickness.” It might originate from the modeling of the connection between the wooden frame and the wooden block part. In the FE models used in these cases, we treated the wooden frame and the wooden block part as a unit, which means that the interfaces nodes are shared with the coupling conditions. However, in the measurement, the block part was simply put on the wooden frame, whereby the wooden block part is not constrained in the wooden frame; one can therefore infer that no structure-borne sound propagation exists between the wooden block part and the wooden frame. To confirm this inference, we conducted additional FE analyses with a model assuming no structure-borne sound propagation at the interface nodes. The wooden blocks have no displacement constraint from wooden frames because they have independent interface nodes. Figures 5(a) and 5(b) show that the FE results were significantly improved for both cases. Differences between FE results and measurements were less than 8 dB in the entire frequency range, and the average differences between FE results and measurements were 2.4–3.4 dB. In addition, the case of 40 mm thickness shows a lower sound reduction index than in the measured results at high frequencies, which is the same trend in the other five cases with additional block part. The FE result for case of the 20 mm thickness shows a larger reduction index than the measured value at 160 Hz–250 Hz frequencies. The reason for the deterioration of the calculation result at around 250 Hz is not clear. However, overall, the agreement is significantly improved with this modeling. We also obtained a slightly better match for the other four cases

with the additional wooden block part. From the results, it can be considered that the possibility of the imposed boundary condition at the interface was different from the actual condition.

Next, we consider the reason for the difference in sound reduction index above 2,000 Hz in all cases except the “All perimeter” case. To examine the reason, we compare SPLs inside the air cavity between FE results and measurements. Note that FE results of acoustic pressure in the inner air cavity were applied at all frequencies as a constant correction value, that was calculated from the differences between the overall value from measurement and that by FE calculation from 100–5,000 Hz in the “Without” case. Figures 6(a)–6(c) present SPLs for the “Width” and “All perimeter” cases as a reference. As expected, the best fit was obtained for the “All perimeter” case, similar to the prediction accuracy of the sound reduction index shown in Fig. 4(b). On the other hand, in the “Width” cases, the FE results agree well with the measurements within an absolute difference of about 9 dB, with an average absolute difference of 2.8–3.1 dB, despite large discrepancies in sound reduction index above 2,000 Hz, as shown in Figs. 4(e) and 4(f). Although the graphs are omitted, even in the “Without” and “Arrangement” cases, for which the discrepancies in sound reduction index are large above 2,000 Hz, the agreement of SPLs between FE results and measurements is better above 2,000 Hz with the average absolute error of 1.9–3.8 dB. From these findings, we inferred that the direct airborne sound transmission across the air cavity was predicted well for all cases. Therefore, the discrepancies in sound reduction index might occur owing to the inaccurate modeling of edge sound transmission between the wooden frame, wooden block part, and rubber sheets. In particular, for the “Without,” “Arrangement,” and “Width” cases, it is indicated that the reproducibility of vibration propagation via the additional wooden block part is low. According to the literature [13], when the depth of the inner air cavity is large, as in the present study, the stiffness of air layers decreases, and the structural propagation from the window frame becomes

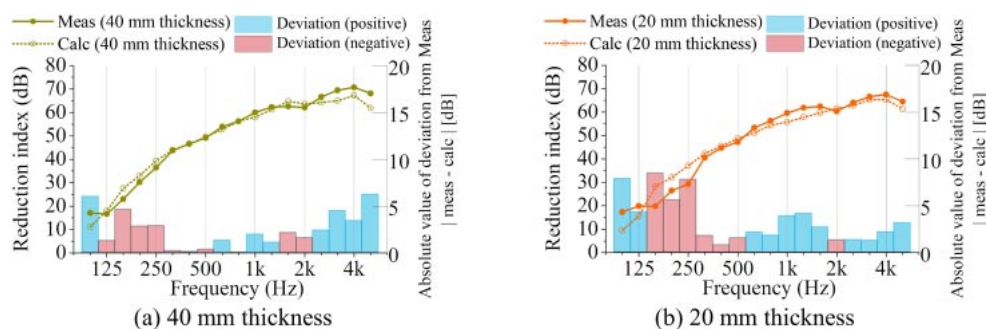


Fig. 5 Sound reduction indices of improved model: simulation and measurement results.

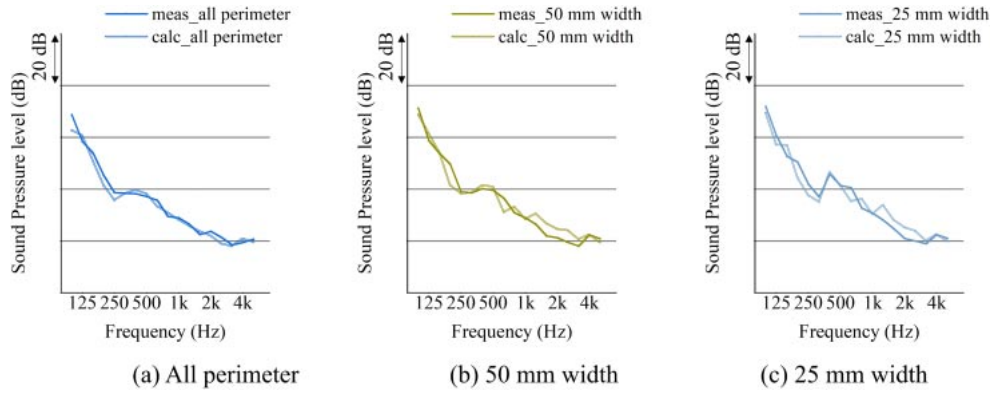


Fig. 6 Sound pressure level at middle microphone (All perimeter, 50 mm width, and 25 mm width).

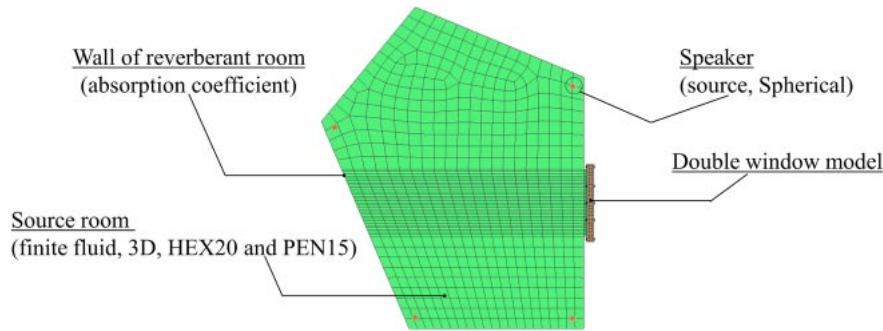


Fig. 7 Finite element model of reverberant room (top view).

dominant. This indicates that the accurate modeling of transmission via a sound bridge would be particularly important for our cases because the inner air cavity depth is 90 mm, which is sufficiently large.

Finally, discrepancies at low frequencies might be attributed to the nonreproduction of the laboratory diffusivity in FE modeling. Because of the reverberant room size of 36.9 m³ volume, it may be impossible to obtain sufficient diffusivity at low frequencies. The sampled random diffuse field component used for FE analysis is a boundary condition to reproduce sufficient diffusivity even at low frequencies. Moreover, it is generally known that at low frequencies, the sound reduction index varies with the test room size [3]. To confirm the effect of room diffusivity, we modeled a source reverberant room for low frequencies. Figure 7 shows the FE model of the reverberant room. The air in the reverberant room was modeled with 3D HEX20 and PEN15, i.e., fifteen-node pentahedron, fluid elements. The element sizes satisfy three elements per wavelength. We assigned the sound absorption coefficient of 0.01 to the inner wall surfaces of the reverberant room. Spherical sound sources emitting a uniform sound pressure at all frequency ranges were placed at the speaker position in the reverberant room. The reduction index was calculated from the average SPL in the reverberant room and the radiation power accordance with JIS A 1441-1. The SPL in

the reverberant room was averaged at five receive points, which are the same as the measured points shown in Fig. 7. Figure 8 shows the calculation results for the “ALL perimeter” and “Without absorption” cases as well as the sampled random diffuse field component results as a representative example. In both cases, with room modeling, sound reduction indices increase compared with the sampled random diffuse field results. Although the improvement can be seen at some frequencies such as 100 and 200 Hz in Fig. 8(a), overall agreements are better for the sampled random diffuse field results in Fig. 8(b). Note that the absorption coefficient used for walls, and sound source characteristics of loudspeakers were not based on the measurement because of the lack of measurement data. Therefore, if those points are considered in the simulations, the prediction accuracy at low frequencies may be improved.

5. CONCLUSION

This study was conducted as a pilot study toward developing an accurate numerical model to predict the sound reduction index of a realistic-scale double window system over a broad frequency range. We used an FE model that discretized only the double windows part. The incident sound source condition was modeled with the sampled random diffuse field. Also, the transmitted sound

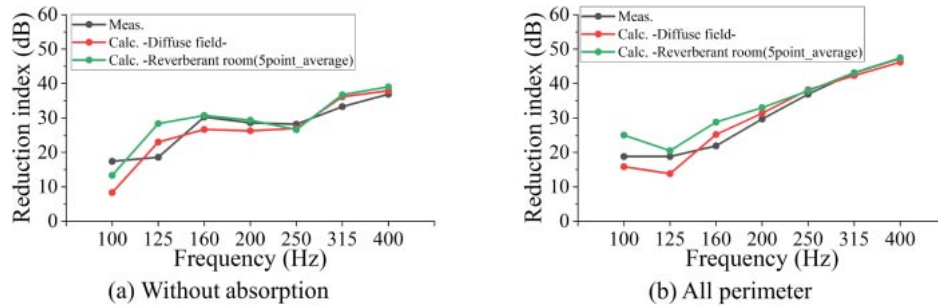


Fig. 8 Sound reduction indices with and without reverberant room.

was calculated using Rayleigh's integral. FE results were compared with measured results for a simple real-scale double window model with and without a frame absorber for a total of eight cases. The findings of the present study are summarized below.

- (1) The best agreement was obtained for the case with the absorption treatment in all the perimeters of the inner air cavity. In that case, the absolute difference from measured sound reduction indices is below 5 dB at all frequency ranges.
- (2) For the "Without," "Arrangement," and "Width" cases, the FE results matched the measured results with an average absolute error of less than 4 dB at frequencies of 160–2,000 Hz. However, large discrepancies appeared at frequencies below 160 Hz and above 2,000 Hz in almost all cases. Also, as a general trend, FE results were smaller than the measured values.
- (3) The "Thickness" case showed the worst agreement with the measured results over a wide frequency range. However, the agreement was significantly improved at 315–5,000 Hz assuming that there is no structure-borne propagation between the wooden frame and the wooden block part.
- (4) In all cases, the FEM-calculated SPLs inside the air cavity were in good agreement with measured values for all frequencies. This indicates that direct sound transmission across the air cavity itself is modeled accurately with the presented FEM model.
- (5) At low frequencies below 160 Hz, modeling the source reverberation room in accordance with actual measurement conditions improved the agreements at some frequencies, but the sampled random diffuse field modeling results show a better fit to measured values at some frequencies.

As shown by the above results, the presented FEM model can predict the sound reduction index of the simplified double windows model quite well under some conditions and limited frequency ranges. On the other hand, sound transmission via structurally connected parts seems to be a cause of the inaccuracy of prediction.

Actual windows with sashes have more complex structurally connected parts. Furthermore, a window has losses and complex vibration in the window frame, unlike a simple panel; thus, the window frame might affect the sound reduction index. Therefore, further study with actual single windows will be necessary for modeling structural sound transmission, window frame vibration, and frame losses in its perimeter.

REFERENCES

- [1] Z. Maekawa, J. H. Rindel and P. Lord, *Environmental and Architectural Acoustics*, 2nd ed. (CRC Press, Boca Raton, 2011), pp. 180–185.
- [2] ISO 10140-1:2016 Acoustics — Laboratory measurement of sound insulation of building elements — Part 1: Application rules for specific products (2016).
- [3] R. W. Guy, A. Demey and P. Sauer, "The effect of some physical parameters upon the laboratory measurements of sound transmission loss," *Appl. Acoust.*, **18**, 81–98 (1985).
- [4] T. Kihlman and A. Nilsson, "The effects of some laboratory designs and mounting conditions on reduction index measurements," *J. Sound Vib.*, **24**, 349–364 (1972).
- [5] A. Corps and D. Soubrier, "Sound transmission loss of glass and windows in laboratories with different room design," *Appl. Acoust.*, **25**, 269–280 (1988).
- [6] A. Tadeu and D. Mateus, "Sound transmission through single, double and triple glazing. Experimental evaluation," *Appl. Acoust.*, **62**, 307–325 (2001).
- [7] P. L. Lewis, "Effect of frame construction on the sound insulation of unsealed windows," *Appl. Acoust.*, **12**, 15–24 (1979).
- [8] W. A. Utley and B. L. Fletcher, "The effect of edge conditions on the sound insulation of double windows," *J. Sound Vib.*, **26**, 63–72 (1973).
- [9] A. London, "Transmission of reverberant sound through double walls," *J. Acoust. Soc. Am.*, **22**, 270–279 (1950).
- [10] L. L. Beranek and G. A. Work, "Sound transmission through multiple structures containing flexible blankets," *J. Acoust. Soc. Am.*, **21**, 419–428 (1949).
- [11] K. A. Mulholland, H. D. Parbrook and A. Cummings, "The transmission loss of double panels," *J. Sound Vib.*, **6**, 324–334 (1967).
- [12] J. L. Davy, "The improvement of a simple theoretical model for the prediction of the sound insulation of double leaf walls," *J. Acoust. Soc. Am.*, **127**, 841–849 (2010).
- [13] J. E. Cambridge, J. L. Davy and J. Pearse, "The sound insulation and directivity of the sound radiation from double glazed windows," *J. Acoust. Soc. Am.*, **148**, 2173–2181 (2020).

- [14] J. L. Davy, M. Fard, W. Dong and J. Loverde, “Empirical corrections for predicting the sound insulation of double leaf cavity stud building elements with stiffer studs,” *J. Acoust. Soc. Am.*, **145**, 703–713 (2019).
- [15] A. Arjunan, C. J. Wang, K. Yahiaoui, D. Mynors, T. Morgan, B. Nguyen and M. English, “Development of a 3D finite element acoustic model to predict the sound reduction index of stud based double-leaf walls,” *J. Sound Vib.*, **333**, 6140–6155 (2014).
- [16] K. A. Dickow, P. G. Domadiya, L. V. Andersen and P. H. Kirkegaard, “A parameter study of coupling properties in finite element models of single-stud double-plate panels,” *Proc. Inter-Noise 2011*, 7 pages (2011).
- [17] A. Arjunan, C. J. Wang, K. Yahiaoui, D. Mynors, T. Morgan and M. English, “Finite element acoustic analysis of a steel stud based double-leaf wall,” *Build. Environ.*, **67**, 202–210 (2013).
- [18] J. Poblet-Puig, R. Vilaseca and A. Rodriguez-Ferran, “Numerical modelling of sound transmission in double walls,” *Proc. EURONOISE 2006*, 6 pages (2006).
- [19] J. Brunskog and P. Davidsson, “Sound transmission of structures. A finite element approach with simplified room description,” *Acta Acust. united Ac.*, **90**, 847–857 (2004).
- [20] F. Løvholt, K. Norèn-Cosgriff, C. Madshus and S. Ellingsen, “Simulating low frequency sound transmission through walls and windows by a two-way coupled fluid structure interaction model,” *J. Sound Vib.*, **396**, 203–216 (2017).
- [21] C. Soussi, W. Larbi and J. Deu, “Experimental and numerical analysis of sound transmission loss through double glazing windows,” *Adv. Acoust. Vib.*, **13**, 195–203 (2019).
- [22] Y. Tsukamoto, Y. Tomikawa, K. Sakagami, T. Okuzono, H. Maikawa and Y. Komoto, “Experimental assessment of sound insulation performance of a double window with porous absorbent materials its cavity perimeter,” *Appl. Acoust.*, **165**, 107317 (2020).
- [23] JIS A 1441-1:2007 Acoustics — Measurement of sound insulation in buildings and of building elements using sound intensity — Part 1: Laboratory measurements (2007).
- [24] ISO 15186-1:2000, Acoustics — Measurement of sound insulation in buildings and of building elements using sound intensity — Part 1: Laboratory measurements (2000).
- [25] F. Fahy and P. Gardonio, *Sound and Structural Vibration*, 2nd ed. (Academic Press, New York, 2007), pp. 303–310.
- [26] MSC software, “Actran 2020 User’s Guide Vol. 1, Installation, Operations, Theory and Utilities” (2020).
- [27] M. Petyt, “Vibration of solids,” in *Introduction to Finite Element Vibration Analysis*, 2nd ed. (Cambridge University Press, New York, 2010), Chap. 5, pp. 148–191.
- [28] M. Petyt, J. Lea and G. H. Koopmann, “A finite element method for determining the acoustic modes of irregular shaped cavities,” *J. Sound Vib.*, **45**, 495–502 (1976).
- [29] J. F. Allard and N. Atalla, “Acoustic impedance at normal incidence of fluids. Substitution of a fluid layer for a porous layer,” in *Propagation of Sound in Porous Media: Modeling Sound Absorbing Materials*, 2nd ed. (John Wiley & Sons, Chichester, 2009), Chap. 2, pp. 15–27.
- [30] J. F. Allard and N. Atalla, “Sound propagation in porous materials having a rigid frame,” in *Propagation of Sound in Porous Media: Modeling Sound Absorbing Materials*, 2nd ed. (John Wiley & Sons, Chichester, 2009), Chap. 5, pp. 73–109.
- [31] Y. Miki, “Acoustical properties of porous materials—Modifications of Delany–Bazley models,” *J. Acoust. Soc. Jpn. (E)*, **11**, 19–24 (1990).
- [32] K. Sakagami, D. Takahashi, H. Gen and M. Morimoto, “Acoustic properties of an infinite elastic plate with a back cavity,” *Acta Acust. united Ac.*, **78**, 288–295 (1993).

APPENDIX

To investigate the effect of the number of samples under the diffuse field incident condition, the reduction indices of 1,250 mm × 1,500 mm single plate glass with various the numbers of incident samples were compared.

For the glass plate 3D HEX20, solid shell elements were used, and the mesh was discretized to satisfy five elements per wavelength for bending waves. The number of divisions in the thickness direction is one. The glass was fixed at 10 mm from the plate edges so that displacement $u_x = u_y = u_z = 0$. The sampled random diffuse field was applied to the incident surface, and the Rayleigh surface was applied to the radiating surface. The maximum sound incident angle is 90 degrees. The energy mean value of the reduction index of 100 samples was assumed to be the true value, and the deviation from the true calculated value was determined for individual cases with different number of samples.

Figure A-1 shows the sound reduction indices for different number of samples, and Figs. A-2(a)–A-2(c) show the deviation from average of 100 samples. From the results, the average deviation from 100 samples is less

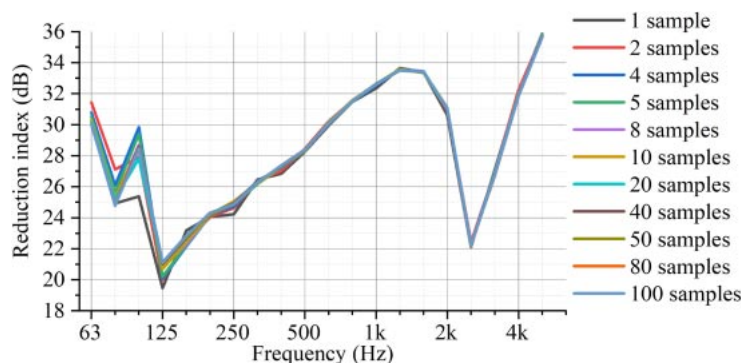


Fig. A-1 Effect of number of input samples on reduction index of simple glass plate.

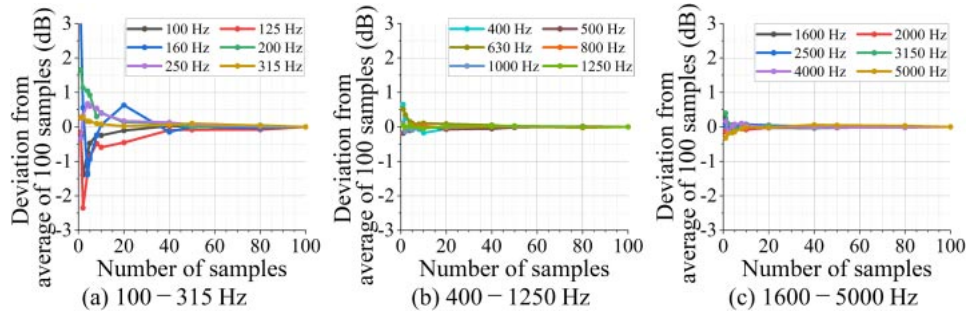


Fig. A-2 Deviation from average of 100 samples.

than 0.25 dB above 315 Hz. The difference was larger at below 200 Hz when a small number of samples were used. However, the differences were less than 0.5 dB when the

number of samples was 10 and 0.25 dB when the number of samples was 40.